Measurements of Rotational Energy Transfer and Quenching in OH $A^2\Sigma^+$, $v'=0$ at Elevated Temperature

M. P. Lee, R. Kienle, K. Kohse-Höinghaus*

DLR-Institut für Physikalische Chemie der Verbrennung, Pfaffenwaldring 38–40, D-70569 Stuttgart, Germany (Fax: +49-711/6862349)

Abstract. Total rotational energy transfer rates have been measured at 1330 K for specific rotational levels in the OH $A^2\Sigma^+$, $v'=0$ state in collisions with H_2O. Rotational levels ranging from $N'=0$ to 15 were studied. Measurements were performed in the post-flame region of a stoichiometric $H_2/O_2/He$ flame operating at 25 mbar. Quenching rates following excitation of individual upper rotational states were also measured. The RET and quenching rates both exhibit monotonic decreases with increasing rotational quantum number.

PACS: 34.00

The hydroxyl radical (OH) has been widely utilized for Laser-Induced Fluorescence (LIF) measurements in reacting gaseous flows. This development has been primarily motivated by the important role of OH as an intermediate species in many chemical reactions, particularly combustion processes. In addition, the strong transition strength of the $A^2\Sigma^+ - X^2\Pi$ electronic transition, the accurate spectroscopic data already measured for this transition and the availability of powerful UV lasers make OH an attractive species for LIF diagnostics. However, difficulties inherent in relating LIF signals to physical properties of interest (such as temperature and concentration) remain important limitations on the applicability of the OH LIF technique for quantitative measurements. In particular, accurate interpretation of LIF measurements requires information on molecular energy transfer rates, including vibrational energy transfer, collisional quenching and rotational energy transfer.

Data on Rotational Energy Transfer (RET) rates are particularly important for the development of quantitative LIF diagnostics. RET acts to redistribute the population in the laser-coupled levels, replenishing the

lower state and depopulating the upper state, and thus delaying the onset of saturation effects. In addition, thermalization due to RET in the upper state reduces the influence of rotational-level-dependent variations in the quenching and spontaneous emission rates on the LIF signal. Finally, rate equation models for energy transfer in LIF, which are required for analysis of experimental strategies and correct interpretation of fluorescence signals, require accurate RET data [1].

Low-temperature RET in the OH A, $v'=0$ and 1 levels has been comprehensively examined [2–7]. Both state-to-state and total RET rates have been measured for a range of rotational levels and a number of species ("state-to-state" implies RET between two specific rotational energy levels, and "total" refers to RET from a specific initial state to all other rotational levels). However, there have been relatively few studies of RET rates in OH at elevated temperature [8–12], the regime of interest for many applications of LIF techniques (including flame studies). In the high-temperature studies which have been performed to date, OH RET has typically been determined by measuring time-resolved or time-integrated LIF spectra and then using modelling approaches to deduce the RET rates. Smith and Crosley [8] measured temporally-integrated fluorescence spectra in an atmospheric-pressure methane/air flame following excitation of transitions to rotational levels in the $v'=0$ vibrational level. Their results, presented as the ratio of the total quenching rate (denoted by Q) to the total RET rate (denoted by R) from the laser-excited state, illustrate a systematic increase in Q/R (the so-called branching ratio) with increasing rotational level. Stepowski and Cottereau [9] studied RET from the $v'=0$ $F_2(7)$ level in a low-pressure C_3H_8/O_2 flame diluted with nitrogen or argon. Temporally-resolved fluorescence spectra were measured at a number of temporal delays following laser excitation, and a three-level model was used to analyze the energy transfer. Mean cross sections for RET and quenching in the flame were determined, and the resultant value of Q/R agreed well with the results of Smith and Crosley [8]. Total RET rates for N_2 and Ar were also determined.

* Now with the University of Bielefeld, Fakultät für Physik, Universitätsstrasse 25, D-33615 Bielefeld, Germany (Fax: +49-521/1062958)

The value of Q/R for the $v' = 0$ $N' = 4$ state measured by Furuya et al. [10] from time-integrated fluorescence spectra in a propane/air flame is also in agreement with the data of Smith and Crosley [8]. Lucht et al. [11] measured RET cross sections for OH in collisions with H_2O in 30 Torr $H_2/O_2/N_2$ flames. Time-resolved LIF spectra were analyzed to determine total RET rates for transfer from the $F_1(1)$, $F_1(4)$, $F_2(5)$ and $F_1(10)$ rotational levels in the $v' = 0$ level. In addition, the multi-level rate-equation model of Chan and Daily [13] was used to determine a set of 34 parameters which could be used to calculate state-to-state RET coefficients. Finally, Zizak et al. [12] measured Q/R for a number of rotational levels in three different hydrocarbon flames using time-integrated fluorescence spectra. In addition to these experimental measurements, theoretical calculations of RET rates have been performed for OH in collisions with Ar [14] and He [15].

From this review, it is clear that additional information on high-temperature OH RET rates are required. Only Stepowski and Cottereau [9] and Lucht et al. [11] have determined species-specific cross sections for OH RET with combustion-relevant collision partners at elevated temperatures. In addition, Stepowski and Cottereau [9] measured rates for only one rotational state, and the scatter in the data of Lucht et al. [11] is too large to conclusively determine whether there is a systematic variation in the RET rate with rotational level. Finally, for the development of accurate scaling-law relations for RET rates which can be used in dynamic models of energy transfer, accurate data over a wide range of rotational levels and temperature is needed. Thus, improved data on OH RET rates are required.

There are two limits in which variations in RET rates have a relatively small influence on linear LIF measurements. First, if the RET from all levels is very rapid compared to the sum of electronic quenching and radiative decay, complete thermalization of the population in the upper state will occur for all excitations, and the details of the RET process become unimportant. However, previous studies have shown that RET in OH does not typically lead to a totally thermal population distribution [8–12]. The second limit where RET variations have little effect on the LIF signal occurs when the dependences of the collisional quenching and radiative decay rates on the laser-coupled upper state are weak. This assumption is often used to simplify interpretation of LIF signals. However, data on room-temperature [16–20] and flame-temperature [21, 22] OH quenching rates and on measured [16, 20] and calculated [23–25] radiative lifetimes indicate that both deexcitation processes are strongly dependent on the upper-state rotational level. Thus, errors in the quantification of LIF can result. This effect is particularly significant in the widely-applied two-line temperature measurement technique, where two different rotational levels are excited and the temperature is determined by relating the signal to the populations in the ground states, as has been shown by Cattolica and Mataga [22]. To date, there has not been a comprehensive study of both OH RET and quenching rates as a function of rotational level at elevated tem-

perature. In the work discussed here, total RET rates for transfer from a single rovibronic level to all other levels due to collisions of OH with H_2O have been measured in a low-pressure flame. Total quenching rates following excitation of individual upper-state rotational levels have also been measured. Rotational levels ranging from $N' = 0$ to 15 in the $v' = 0$ vibrational level of OH have been studied. For this study, a novel technique has been developed for the measurement of RET and quenching rates, and this technique will be discussed in detail below.

1 Theory

Laser-induced fluorescence can be analyzed using a rate equation approach [26, 27]. In general, a multi-level model which explicitly includes all rovibronic states is required for accurate interpretation of fluorescence signals [1, 13, 28]. For the study discussed here, a simplified rate equation model is sufficient for analysis of the temporally dependent fluorescence signal. This is because we are only interested in determining the total RET rate from a particular initial upper state to all other upper states, and thus the details of the energy transfer within the latter group of collisionally-populated states and within the ground state are unimportant. The model is illustrated schematically in Fig. 1. In the upper state, the energy levels can be grouped into two categories, consisting of the energy level directly populated by the laser excitation (denoted by L) and the energy levels which are collisionally populated via RET (denoted by j). Energy transfer processes considered in this model include laser excitation and stimulated emission (with rates given by $b_{1L}I_v$ and $b_{L1}I_v$), rotational energy transfer from the laser-coupled state (R_{Lj}), back-transfer from the collisionally-populated states (R_{jL}), RET within the ensemble of collisionally-populated levels (R_{ji} and R_{ij}, $i, j \neq L$), collisional quenching (Q_L and Q_j) and spontaneous emission (A_L and A_j). The rate equations for the time-dependent populations N_L and N_j are

$$dN_L/dt = b_{1L}I_vN_1 - \left(b_{L1}I_v + Q_L + A_L + \sum_{j \neq L} R_{Lj}\right)N_L$$
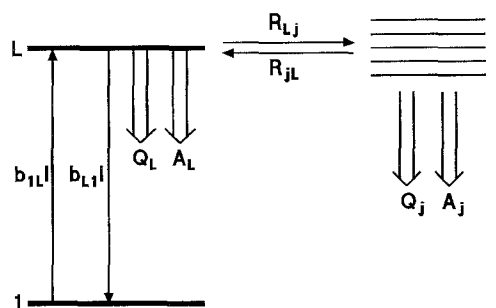
$$+ \sum_{j \neq L} R_{jL}N_j, \tag{1}$$

Fig. 1. Energy-level model used for data analysis

$$dN_j/dt = R_{Lj}N_L - \left(Q_j + A_j + R_{jL} + \sum_{i \neq j,L} R_{ji} \right) N_j$$

$$+ \sum_{i \neq j,L} R_{ij} N_i. \tag{2}$$

Summing (2) over j removes the terms related to RET within the ensemble of collisionally populated states. The result is

$$dN_C/dt = R_L N_L - \sum_{j \neq L} (Q_j + A_j + R_{jL}) N_j, \tag{3}$$

where N_C denotes the population in the ensemble of states which undergo RET with the laser-coupled level, i.e.,

$$N_C(t) \equiv \sum_{j \neq L} N_j(t), \tag{4}$$

and where R_L (the total RET rate) is defined as

$$R_L \equiv \sum_{j \neq L} R_{Lj}. \tag{5}$$

Ideally, the total RET rate R_L from the directly laser-populated level to all other levels can be measured by directly observing the decay of the population in the laser-excited level N_L. Unfortunately, such measurements present several practical difficulties. The RET is typically very fast, especially in the relatively high densities encountered in flames. During the duration of the laser pulse, the population in the laser-coupled level is governed by the laser excitation, and so direct measurement of the RET rate during this time period is not possible. The rapid RET results in significant transfer to the collisionally-populated levels, and thus once the laser excitation ends the decay of the laser-coupled level is influenced by back-transfer. Even if these problems are avoided (e.g., by using a short-pulse-length laser), the decay from the laser-coupled level is influenced by the rate of quenching from this state. Direct measurement of this state-specific quenching rate is not possible due to the thermalization of the population by RET.

The total RET rate R_L can instead be determined by solving (3) and integrating from initial time t_0 (usually taken to be the start of the laser pulse) to final time t. The result is

$$R_L = \left[1/\int_{t_0}^t N_L(t')\, dt' \right] \left\{ [N_C(t) - N_C(t_0)] \right.$$

$$\left. + \sum_{j \neq L} (Q_j + A_j) \int_{t_0}^t N_j(t')\, dt' + \sum_{j \neq L} R_{jL} \int_{t_0}^t N_j(t')\, dt' \right\}. \tag{6}$$

From this equation it can be seen that R_L is initially dominated by the first term in (6), which represents the rate of transfer from the laser-excited level into the RET-populated states. With increasing time, contributions from collisional quenching and radiative decay, represented by the second term in (6), and back-transfer, the third term in (6), become significant. The second term can be approximated from the exponential decay (with

time constant τ) of the broadband fluorescence from the ensemble of upper states following excitation of state L via the equation

$$\sum_{j \neq L} (Q_j + A_j) \int_{t_0}^t N_j(t')\, dt' \approx (1/\tau) \int_{t_0}^t N_C(t')\, dt'. \tag{7}$$

Equation (6) can then be rewritten

$$R_L = \left[1/\int_{t_0}^t N_L(t')\, dt' \right] \left\{ [N_C(t) - N_C(t_0)] \right.$$

$$\left. + (1/\tau) \int_{t_0}^t N_C(t')\, dt' + \sum_{j \neq L} R_{jL} \int_{t_0}^t N_j(t')\, dt' \right\}. \tag{8}$$

In practice, all components of the first two terms can be measured experimentally. Only the term related to back-transfer cannot be determined experimentally. In addition, the magnitude of the back-transfer term is small near the beginning of the laser pulse (i.e., near time t_0). Thus, the RET rate can be determined by measuring the first two terms and extrapolating back to time t_0, i.e.,

$$R_L = \lim_{t \to t_0} \left\{ [N_C(t) - N_C(t_0)] \right.$$

$$\left. + (1/\tau) \int_{t_0}^t N_C(t')\, dt' \right\} / \int_{t_0}^t N_L(t')\, dt'. \tag{9}$$

A similar approach has previously been applied for the measurement of room-temperature state-to-state RET rates. Note that this measurement technique is not influenced by the details of the excitation process, and, in particular, it is independent of the degree of saturation of the absorption transition.

2 Validation of the Measurement Technique

The measurement technique can be examined in more detail with the aid of calculations. These computations were performed using a dynamic multi-level rate equation model [1] incorporating approximately 50 rotational levels in the A, $v' = 0$ state of OH. A 15 ns long laser pulse was assumed to excite isolated rovibronic transitions in the A–X (0, 0) band. In order to simulate a realistic experimental situation, accurate energy transfer data were required. The gas composition which would be encountered in a low-pressure $H_2/O_2/He$ flame at 1330 K was computed using a 1–D flame code [29]. The rates for quenching were calculated using cross sections from Garland and Crosley [30] (for H_2O, H_2 and O_2) and Cattolica and Mataga [22] (for H atoms). A complete matrix of state-to-state RET rates was generated using the combination of available RET data and the Energy-Corrected Sudden-Power (ECS–P) scaling law. This scaling law allows extrapolation of measured low-T RET rate coefficients [6, 7] to a wide range of rotational levels and temperatures, and the validity of the extrapolation has been confirmed by comparison with measured rates [11] (a detailed discussion of the scaling law will be presented in a future publication [31]). At the conclusion of the
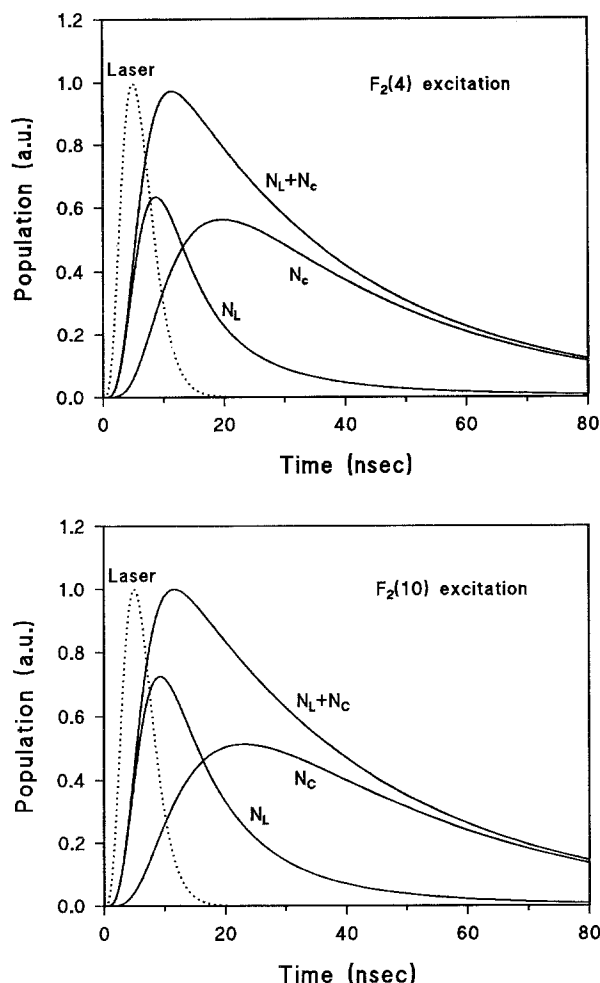
Fig. 2. Model calculations of fluorescence transients for excitation of the $F_2(4)$ and $F_2(10)$ levels. These computations have been performed using a full multi-level rate equation model [1]. A realistic laser temporal profile (also shown) has been used for the computation
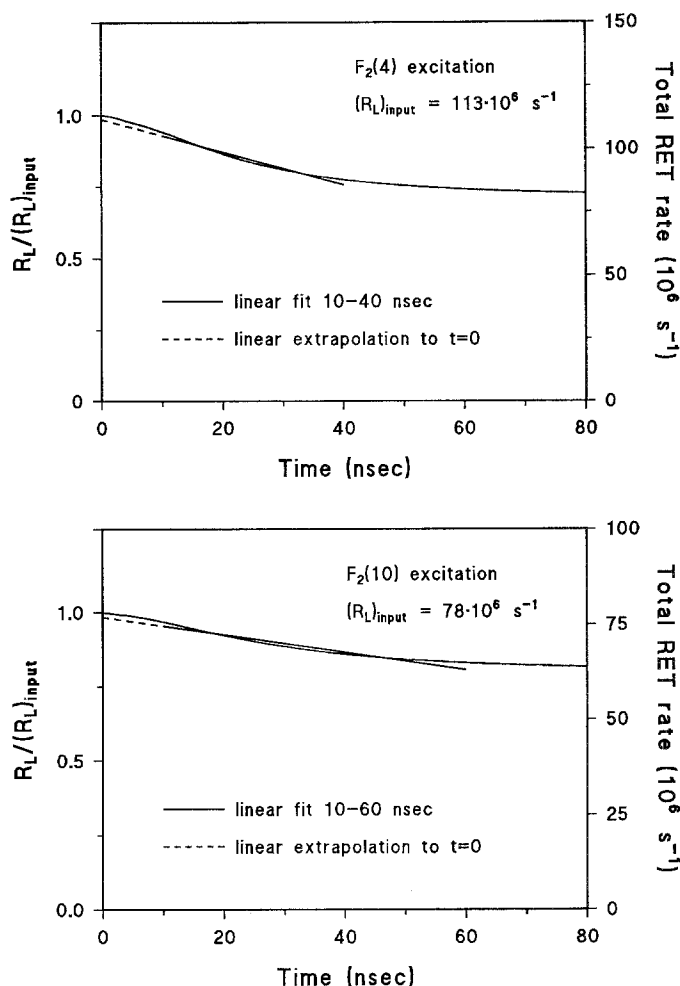

Fig. 3. Model calculations illustrating the accuracy of the extrapolation technique for determination of the RET rate. Results are shown for the $F_2(4)$ and $F_2(10)$ levels. Note the reduced influence of back-transfer for the $F_2(10)$ state

study presented in this paper, the measured rates for quenching and total RET for OH in the investigated $H_2/O_2/He$ flame have been used to improve the accuracy of the scaling law fit parameters; note, however, that this refinement is not significant for the test of the RET measurement method.

For the validation of the proposed measurement technique, a computational experiment was performed. Following laser excitation, the time-dependent populations for each rotational level in the rotational manifold were computed using the multi-level rate equation model, and the corresponding transient populations in the laser-coupled state and in the states populated by RET were calculated. These transients were then analyzed (as they would be in an actual experiment) using (9) to determine the "measured" RET rate, and this rate was compared to the initially input value. Agreement between the initially input and "measured" rates was taken as confirmation of the accuracy of the proposed measurement technique. Computed transient populations are shown in Fig. 2 for excitation of the $F_2(4)$ and $F_2(10)$ rotational levels. The decay rate $(=1/\tau)$ of the total upper-state

population $N_L(t) + N_C(t)$ can be combined with the time-dependent populations $N_L(t)$ and $N_C(t)$ and input into (9) to determine the RET rate. This result is shown in Fig. 3 as the ratio of the "measured» RET rate to the initially input rate. Comparison of the results for the two different excitations is illustrative. The slope of the linear fit for the extrapolation for the $F_2(4)$ state is about twice as high as the slope for the $F_2(10)$ extrapolation. This is a consequence of the fact that the magnitude of back-transfer is greater for the $F_2(4)$ excitation than for $F_2(10)$. The back-transfer is greater for this state because the RET will tend to produce a thermal population distribution centered around $N' = 4$ (for the input temperature of 1330 K). Note that the RET rate determined via this method agrees very well with the input rate at time t_0 for both excitations. Note also that there is a relatively long time range over which an accurate extrapolation to time t_0 can be performed, and that the optimal time interval may differ for each excitation due to the varying influences of RET, quenching and back-transfer. The rate equation model has been used to determine the optimal interval for the linear fit for each rotational level which was

studied, and these intervals were used for analysis of the experimental data.

The proposed measurements technique was tested with the full multi-level model for a range of experimental conditions. Parameters which were varied included the rotational level under investigation (from $N' = 0$ to 15), laser temporal profile (from instantaneous excitation to very long laser pulses), laser pulse energy (from weak excitation to complete saturation) and branching ratio (from low to high Q/R). For all of the conditions which were examined, the measurement procedure described here was shown to permit accurate determination of RET rates. In particular, the accuracy of linear extrapolation to time t_0 (as opposed to extrapolating with a nonlinear approach) was demonstrated. These results confirm the accuracy of the measurement technique.

3 Experimental Setup

A schematic of the experimental setup is shown in Fig. 4. A Nd:YAG-based dye laser system (Quanta-Ray DCR/PDL/Wex) operating on sulforhodamine 101 laser dye produced light at 308 nm which was suitable for excitation of single rotational transitions in the OH $A-X$ (0, 0) band. The laser linewidth and UV pulse energy were approximately 1 cm^{-1} and 1 mJ/pulse, respectively. The unfocussed laser beam (diameter ≈ 3 mm) was propagated into the low-pressure burner at a height of 48 mm above the burner surface (in the post-flame region), and the fluorescence was observed at right angles to the laser path. A polarization scrambler was used to remove the influence of polarization on the spatial distribution of the fluorescence. Light baffles and 10°-angle windows were used on the laser entrance and exit to reduce laser scattering.

The flat-flame burner (McKenna Products, 60 mm diameter, brass plate) was operated with a stoichiometric mixture of H_2 and O_2 diluted with 50% He (flow rates 2.67 slm H_2/1.33 slm O_2/4 slm He) at a pressure of 25 mbar. Gas flows were metered using calibrated flow controllers (Tylan FC280S). A feedback-controlled iris

FD: frequency doubler
PB: Pellin Broca prism
PS: polarization scrambler
PM: photomultiplier
F : filter

Fig. 4. Experimental setup

valve (Balzers IB040) was used to maintain constant pressure in the burner. The pressure in the burner was stable to within 0.1 mbar.

Several criteria were considered in the selection of flame conditions. A stoichiometric H_2/O_2 flame provided simple flame chemistry which could easily be modelled with a 1–D flame code. Modelling permits estimation of species concentrations, which can be used to convert energy transfer rates into cross sections. In addition, it was necessary to utilize as low a pressure as possible, in order to lower the energy transfer rates to within the temporal resolution of the detection system. The minimum pressure was limited by two factors: flame stability and increasing concentrations of radical species, particularly H atoms. The addition of 50% He to the flame permitted reduction of the H_2O concentration (and thus the RET rate), while maintaining sufficient pressure for flame stabilization. The choice of He as diluent was dictated by its relatively small cross sections for RET and quenching. One drawback of the large concentration of buffer gas is that collisions with He do contribute a non-negligible amount of RET. The influence of He RET on the determination of H_2O RET rates will be discussed later.

Determination of the RET rate with the method described in the previous section necessitates monitoring of the ensemble of states which constitute the population N_C. Unfortunately, direct measurement of the population in these states is not possible because the fluorescence from these levels is spectrally overlapped with the signal from the laser-coupled level. This has motivated the development of a novel technique for the determination of N_C. This population can be determined from two measurements: first, by measuring the population in the laser-excited level ($\approx N_L$) via detection of single-line fluorescence; and second, by measuring the population in the entire upper state ($\approx N_L + N_C$) via detection of broadband fluorescence. Then, the time-dependent population N_C can be obtained simply by subtracting the population in the laser-coupled level from the total population. It should be noted that the narrowband and broadband fluorescence signals are typically registered with different detection systems, and thus calibration of these systems with respect to each other is required in order to directly relate the signals. The calibration procedure will be discussed in the next section.

In the broadband fluorescence channel, the spectrally-integrated LIF signal was collected with two lenses and focussed onto a photomultiplier. In the narrowband channel, two mirrors were used to rotate the fluorescence image by 90°, and a lens focussed the fluorescence onto the entrance slit of a monochromator (Jobin-Yvon HR640, 640 mm focal length) equipped with an appropriate grating (2400 lines/mm, blazed for 170–500 nm). Slit heights and widths were 2 mm and 50 μm, respectively, resulting in a triangular slit function with a FWHM of approximately 4 cm^{-1}, suitable for detection of isolated transitions. A photomultiplier was mounted on the monochromator exit slit. Calibrated UV neutral-density filters (Melles Griot) were used in both channels to prevent saturation of the photomultipliers.
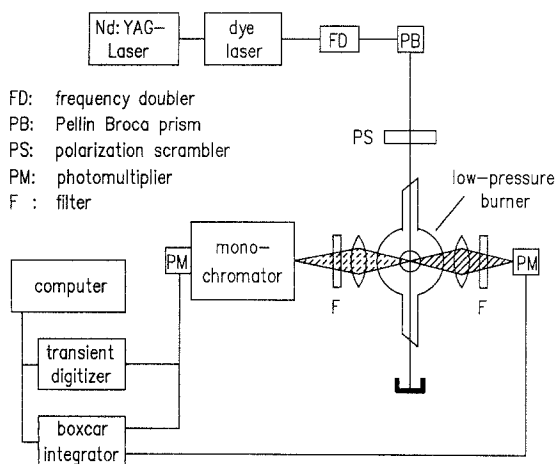
For the registration of time-resolved fluorescence transients, high temporal resolution was required. A high-speed PMT (Hamamatsu H3378–01) was utilized in combination with a high-speed amplifier (Tektronix 7A19) and a transient digitizer (Tektronix 7912AD). The resolution of the complete detection system was measured with a picosecond laser system (Heidelberg University) and was determined to be approximately 1–2 ns. Typically, several thousand single-shot transients were acquired and averaged to determine one time-resolved transient. For the measurement of the broadband fluorescence decay, a relatively constant detection efficiency was very important. If the detection efficiency varies significantly over the wavelength range of the fluorescence emission, preferential detection of elevated or low-lying rotational levels may occur. This effect may influence determination of the fluorescence decay rate. The detection efficiency of the broadband fluorescence channel was checked and was verified to be roughly constant over the wavelength range of interest.

For time-integrated fluorescence measurements, broadband and narrowband fluorescence signals were detected with photomultipliers and the resulting fluorescence signals were temporally integrated and averaged with boxcar averagers connected to a computer interface (Stanford Research Systems SR250/SR245). For acquisition of fluorescence spectra, the monochromator was scanned at 0.0025 nm/s and 30-sample averaging was used. The boxcar gate widths were approximately 80 ns. Active baseline subtraction (achieved by double triggering the boxcar averager and alternating the signal polarity) was used to remove the influence of baseline drift on the fluorescence spectra. A photodiode observing the laser scattering was used as the trigger source for the data acquisition system.

The fluorescence spectra were measured by scanning the monochromator wavelength over a wide range, typically on the order of 10 nm. Over this wavelength range, the detection efficiency of the narrowband detection system changed, primarily due to variations in the monochromator grating efficiency and photomultiplier sensitivity. Accurate interpretation of the fluorescence spectra requires correction for this effect. The spectral efficiency of the narrowband detection system was measured by placing a deuterium lamp at the measurement location and scanning the monochromator over the same wavelength range as the OH spectra. The well-known D_2 spectrum [32] was then used to accurately profile the detection system. The results illustrate that over the range of the fluorescence spectra scans, the detection efficiency varied linearly by roughly 6%.

4 Experimental Procedure

Measurement of RET rates were performed in several steps. First, time-resolved broadband ($\approx N_L + N_C$) and narrowband ($\approx N_L$) fluorescence transients were successively acquired. Then, a fluorescence spectrum was measured by scanning the monochromator wavelength and recording the narrowband signal. The spectral loca-

tion of an isolated transition originating from the laser-coupled level was identified, and repeated monochromator scans over this line were also performed. During the scans of the spectrally resolved fluorescence, the broadband LIF signal was measured and was used to normalize the narrowband signal for variations in experimental parameters (e.g., fluctuations in laser power, detuning of the laser from linecenter, etc.). The temporal position and duration of the boxcar gate relative to the fluorescence signal were also recorded. The fluorescence scans were corrected for baseline offset, reference signal fluctuations and detection efficiency variations. The corrected fluorescence signal for the single transition originating from the laser-populated level was then spectrally integrated and combined with the well-known Einstein coefficients [25] to determine the sum of the fluorescence intensities for all transitions originating from this level. The complete fluorescence spectrum was also spectrally integrated, and the ratio of the fluorescence from the laser-coupled level to the total fluorescence intensity was computed. This result was then used to relate the narrowband and broadband transient measurements, by temporally integrating both transients over the duration of the boxcar gate width. Finally, the narrowband transient could be subtracted from the broadband transient in order to determine the time-dependent population in the collisionally-populated level. The decay rate from the entire upper state (the sum of quenching and spontaneous emission) was also determined from the broadband transient. These results were then combined with (9) to determine the RET rate.

Acquisition of narrowband fluorescence required identification of isolated transitions for both excitation and also for observation of the fluorescence originating from the laser-coupled level. The OH spectrum [33] was carefully examined to identify spectrally separated transitions in the (0, 0) band. The excitation and detection strategies used in this experiment are presented in Table 1.

Fluorescence trapping may cause measurement errors. This effect was examined by exciting to the $F_2(4)$ state in A, $v' = 0$. This state was chosen for study because the $N'' = 4$ rotational level has maximum population at the measurement temperature of 1330 K, and thus the largest influence of fluorescence trapping will be observed for this level. Fluorescence transitions originating from this state were detected using the narrowband detection system. A narrow temporal gate (≈ 1 ns duration)

Table 1. Isolated absorption and fluorescence transitions in the OH A–X (0, 0) band

Level	Absorption	Fluorescence
$F_1(0)$	$P_{12}(1)$	$P_{12}(1)$
$F_2(4)$	$S_1(2)$	$R_2(3)$
$F_2(5)$	$S_1(3)$	$R_2(4)$
$F_2(7)$	$S_1(5)$	$Q_2(7)$
$F_2(10)$	$S_1(8)$	$Q_2(10)$
$F_2(12)$	$S_1(10)$	$P_2(13)$
$F_2(15)$	$R_2(14)$	$P_2(16)$

was positioned at the initial rise of the laser pulse to avoid detection of fluorescence from overlapping collisionally-populated levels. The ratio of fluorescence signals for the different transitions was then compared with ratios determined from the Einstein A coefficients [25]. In the limit of no fluorescence trapping, the measured and calculated ratios chould agree. The results illustrated that for the ratio of the weakest to the strongest rotational transitions [$Q_{21}(4)$ compared to $Q_2(4)$], trapping of the fluorescence was less than 10%. For excitation of other rotational levels, this effect should be reduced. Thus, fluorescence trapping is not expected to have a significant influence on the measurement accuracy.

Elastic scattering of laser light can also influence the measurement. There are two primary sources for laser scattering: scattering from the burner walls and windows, and Rayleigh scattering from the gas flow. The magnitude of the Rayleigh scattering was observed to be negligible. In contrast, scattering from burner surfaces was significant. The magnitude of the scattering signal was significantly reduced by installing 10° windows and light baffles in the laser entrance and exit paths. For most of the studies performed here, the scattering signal was thus reduced to very low levels. In general, no correction of the narrowband signal was necessary, and only small correction of the broadband signal for laser scattering was required. However, for study of $F_1(0)$ rotational level, where the narrowband fluorescence signal had to be detected via the same transition as the excitation, the laser scattering signal was larger. The influence of this effect on the determination of the RET rates is discussed in Sect. 6.

5 Results

5.1 Energy Transfer Rates

Representative temporally integrated fluorescence spectra (gate width = 90 ns) acquired following excitation of two rotational levels, $F_2(4)$ and $F_2(10)$, are shown in Fig. 5. The locations of transitions originating from the laser-coupled level are indicated by the starred symbols. Differences in the spectra are caused by variations in the ratio of the RET rate to the deexcitation rate from the excited electronic level. For low rotational levels such as $F_2(4)$, rapid RET acts to efficiently distribute population throughout a wide range of rotational levels. In contrast, in the spectrum acquired following excitation of the $F_2(10)$ level, the slower RET relative to the sum of radiative decay and electronic quenching leads to a larger fraction of the LIF signal originating from the directly laser-coupled level.

Time-resolved fluorescence transients resulting from excitation of the $F_2(4)$ and $F_2(10)$ states are shown in Fig. 6. The narrowband and broadband transients (denoted by N_L and $N_L + N_C$, respectively) were measured directly and were related via the fluorescence spectrum. The population N_C in the ensemble of collisionally-populated states was then deduced from these results. These transients exhibit the expected characteristics.
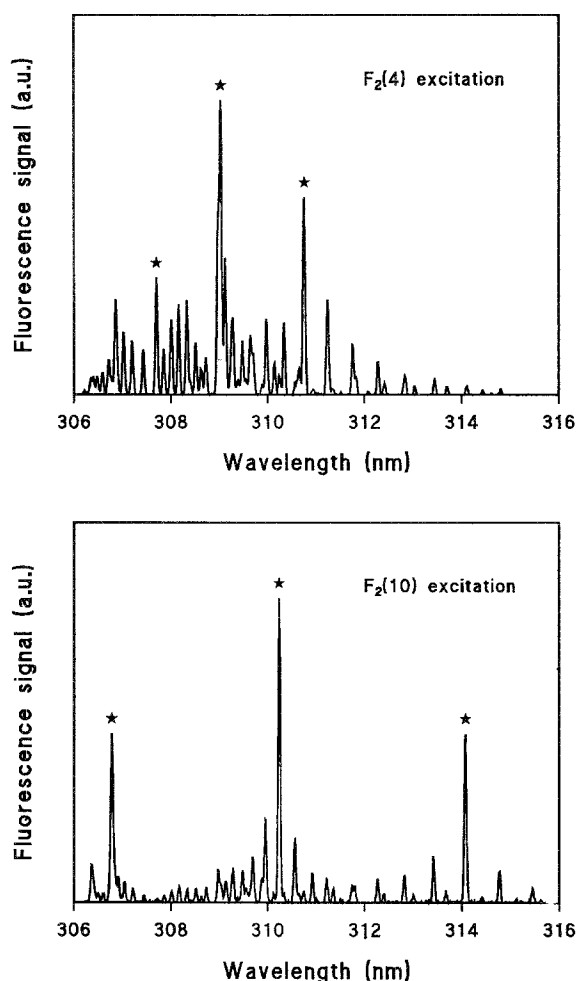

Fig. 5. Fluorescence spectra acquired following excitation of the $F_2(4)$ and $F_2(10)$ levels. The symbols indicate transitions originating from the laser-coupled levels

During the duration of the laser pulse (approximately 10 ns), the laser-coupled state shows a rapid rise in population. Once the laser pulse ends, the population in this state begins to decay, primarily due to RET and collisonal quenching. In contrast, the total population in the upper state shows a slower decay, with a rate characterized by the rotationally-averaged quenching rate. The population in the collisionally-populated levels rises initially due to RET, and then decays due to collisional quenching and back-transfer. Note also the good qualitative agreement between the computed and the measured transients shown in Figs. 2 and 6, respectively.

Rotationally averaged quenching rates can be determined directly from the decay of the broadband fluorescence signal. For each transition, the fluorescence signal was plotted on a semilog scale and a linear fit was performed over the time period from 15 ns (well after the end of the laser pulse) to 80 ns, corresponding to an interval of approximately two decay lifetimes. The quenching rates could then be determined by subtracting the radiative decay rate [25] from the total decay rate. Note that the rotationally averaged radiative lifetime which results from the partial thermalization of the rotational population should be used in this calculation. However,
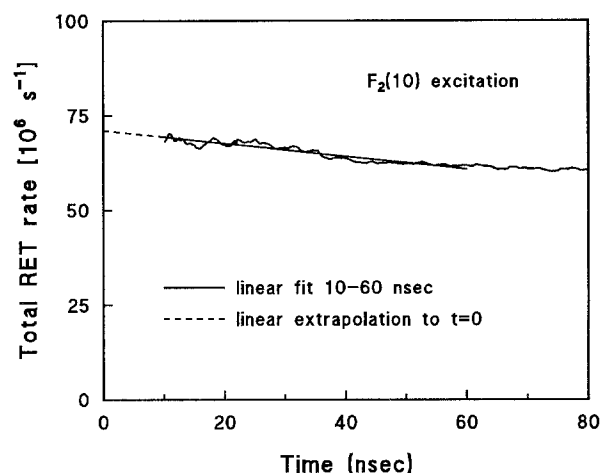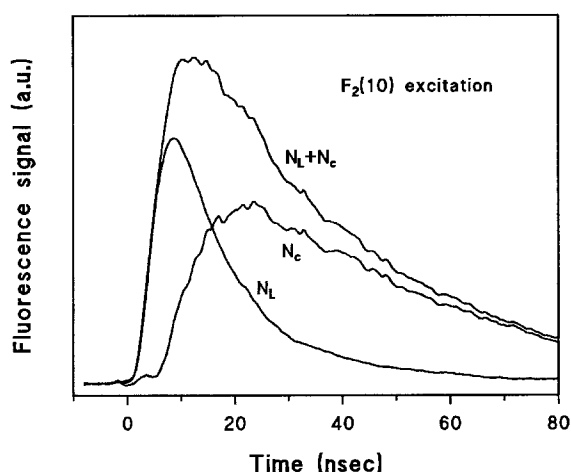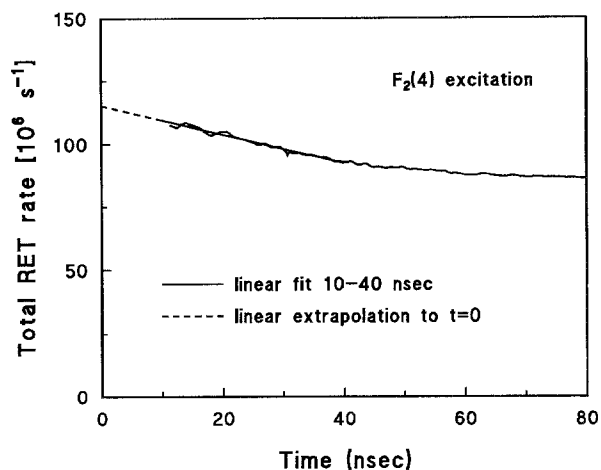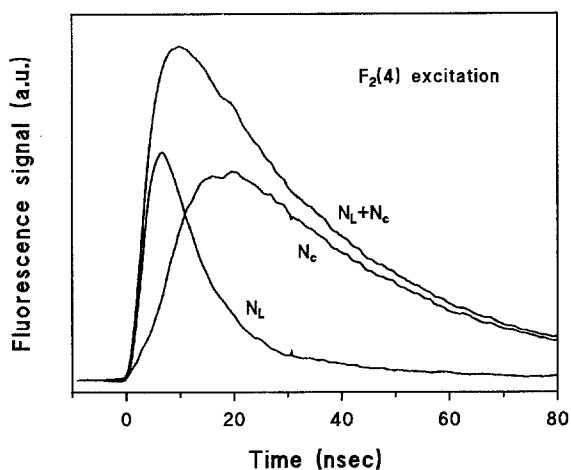
Fig. 6. Transient populations resulting from excitation of the $F_2(4)$ and $F_2(10)$ rotational level. $t = 0$ ns corresponds to the beginning of the laser pulse

Fig. 8. Extrapolation back to time 0 to determine the measured RET rates for the $F_2(4)$ and $F_2(10)$ levels
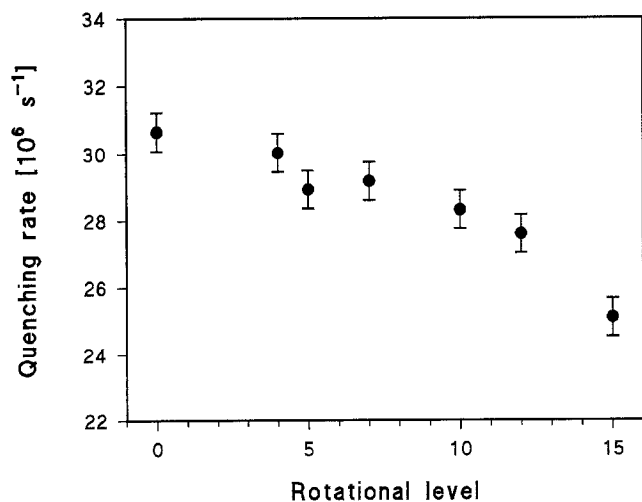

Fig. 7. Rotationally averaged quenching rates as a function of the initially excited rotational level

it is not possible to determine this rate directly, and thus the radiative lifetime of the directly laser-coupled state is used as an estimate of this rate. For the flame conditions in this study, the radiative emission rate is small compared to the quenching rate (always $< 5\%$), and thus this approximation causes no significant error. The resultant quenching rates are plotted as a function of rotational level in Fig. 7. The monotonic decrease of the quenching rate with increasing rotational level (18% from $N' = 0$ to 15) is consistent with previous flame-temperature measurements [21, 22].

Fluorescence transients of the type shown in Fig. 6 can be combined with (9) to determine the RET rate. The results for the $F_2(4)$ and $F_2(10)$ states are shown in Fig. 8. For the $F_2(4)$ level, the time period from 10 ns to 40 ns has been used for the extrapolation, while 10 ns to 60 ns has been used for the $F_2(10)$ level. Deviations from a constant RET rate are caused by the influence of rotational back-transfer on the determination of the rate. Note, however, that the long time period over which the RET rate decreases approximately linearly permits accurate extrapolation back to time t_0 to determine the RET rate. Errors resulting from the extrapolation will be discussed below.
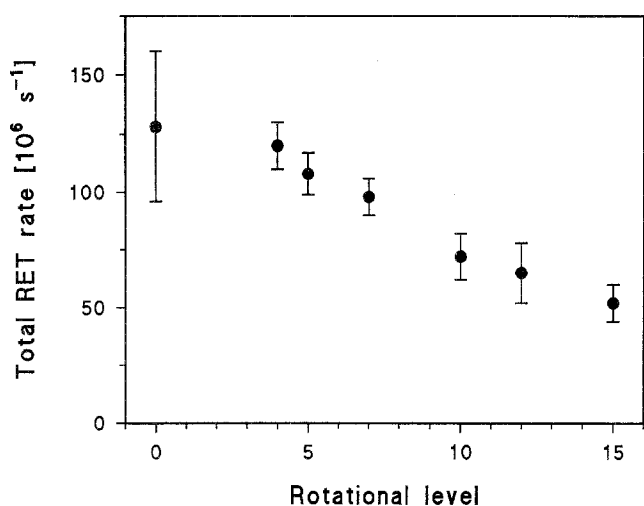
Fig. 9. Total RET rates as a function of rotational level

The resultant total RET rates as a function of rotational level are plotted in Fig. 9. A 60% decrease in the RET rate from $N' = 0$ to $N' = 15$ is observed. Note that the RET rate decreases more than the quenching rate with increasing rotational level. This trend is consistent with previous measurements of the branching ratio Q/R [8, 10, 12]. Direct comparison of the branching ratio measured here with previous results is not possible in view of the varying flame compositions utilized in these studies.

It is interesting to attempt to relate the measured rates for RET and quenching to collisional absorption linewidths in OH [34]. Mechanisms which may contribute to OH line broadening include RET in the upper and lower states, quenching from the upper state, and energetically elastic dephasing collisons. Assuming that X-state RET occurs at the same rate as A-state RET and ignoring the effect of elastic collisions results in a linewidth for the (0, 0) $Q_2(5)$ transition of 0.09 cm^{-1}/atm. In comparison, Rea et al. [35] have measured a FWHM for broadening of OH by H_2O of 0.16 cm^{-1}/atm at 1620 K. There are two possible causes for this apparent discrepancy: first, the X-state RET may be significantly faster than the RET in the A-state; and second, dephasing collisions may have an important influence on OH line broadening. From this brief examination it can be concluded that RET and quenching in the A state of OH contribute a nonnegligible amount to broadening of OH linewidths. However, other mechanisms such as X-state RET or elastic dephasing may have an even more significant influence on OH collisional broadening, and attempts to determine OH linewidths from measured rates for A-state RET and quenching will most likely result in erroneously low values.

As can be seen from Figs. 7 and 9, accurate measurements of total RET and quenching rates have been performed. The combination of the large number of rotational levels examined and the high precision of the measurement permits observation of systematic variations in the rates with rotational energy. Furthermore,

these high-temperature results are consistent with extrapolations of low-temperature RET data performed using the ECS–P scaling law [31]. In contrast, the conversion of these energy transfer rates to collision cross-sections is subject to additional sources of systematic error (e.g., incorrect flame composition). These error sources will be discussed below.

5.2 Energy Transfer Cross Sections

Conversion of the measured RET rates into cross sections and estimation of the contribution of He to the RET rate requires knowledge of the temperature and chemical composition at the measurement location. The temperature profile along the burner centerline was measured by detecting the fluorescence signal following excitation of a series of rotational transitions in the OH A–X (1, 0) band at several locations along the flow centerline and using Boltzmann plots to determine the temperature at each point. The resulting centerline temperature profile was input into a 1–D flame code [29] in order to determine the chemical composition along the flame centerline. The temperature at the measurement location was thus determined to be $T = 1330 \pm 30$ K, and the species concentrations were $\chi(H_2O) = 26.3\%$, $\chi(OH) = 0.8\%$, $\chi(H_2) = 5.1\%$, $\chi(O_2) = 3.4\%$, $\chi(H) = 9.3\%$, $\chi(O) = 1.3\%$ and $\chi(He) = 53.8\%$. Details of the temperature measurement and flame code calculations will be discussed in a future paper on the measurement of high-temperature RET and quenching rates in the OH $(A, v' = 1)$ state.

Examination of the flame composition and previously reported values for rotational energy transfer rates indicates that the only species which contribute significantly to the RET are H_2O and He. Jörg et al. [15] have calculated state-to-state He rate coefficients for a wide range of temperatures and rotational levels up to $N' = 5$. These calculations agree well with experimental data on He RET at 300 K [4]. Their values have been used to estimate the contribution of He to the RET, and the measured RET rates before and after correction for the contribution of He are shown in Table 2. In general, the He RET rate is quite large for the $F_1(0)$ state and de-

Table 2. Total RET rates and cross sections vs rotational state for the OH A, $v' = 0$ level in collisions with H_2O at 1330 K. Corrected data account for the contribution of He to the RET. For the states for which no data on He RET is available, it is estimated that collisions with He will contribute less than 10% of the RET rate

Level	Rate [s^{-1}]	Corrected rate [s^{-1}]	σ [Å^2]	Corrected σ [Å^2]
$F_1(0)$	$128 \pm 32 \times 10^6$	$85 \pm 32 \times 10^6$	199 ± 50	132 ± 50
$F_2(4)$	$120 \pm 10 \times 10^6$	$97 \pm 10 \times 10^6$	187 ± 16	151 ± 16
$F_2(5)$	$108 \pm 9 \times 10^6$	$91 \pm 9 \times 10^6$	168 ± 14	142 ± 14
$F_2(7)$	$98 \pm 8 \times 10^6$		153 ± 12	
$F_2(10)$	$72 \pm 10 \times 10^6$		112 ± 16	
$F_2(12)$	$65 \pm 13 \times 10^6$		101 ± 20	
$F_2(15)$	$52 \pm 8 \times 10^6$		81 ± 12	

creases rapidly with increasing rotational level (faster than the decrease in the total RET rate). Correction of the measured RET rates for the influence of He is not possible for rotational levels above $N' = 5$, but in view of the rapid decrease in the He RET rate with increasing N' we anticipate that collisions of OH with He will contribute less than 10% of the total RET for these states. The calculated flame composition can be used to extract RET cross sections for collisions of OH with H_2O, and these values are also shown in Table 2. Note that collisions with H atoms may also contribute to the RET. No data is available on H atom RET, however, we expect that the contribution will be relatively minor because of the small mass of this species.

Cross sections for RET in the A, $v' = 0$ state of OH at elevated temperatures for collisions with H_2O have previously been measured only by Lucht et al. [11]. Their results were $\sigma[F_1(1)] = 110 \pm 30$ Å^2, $\sigma[F_1(4)] = 170 \pm 60$ Å^2, $\sigma[F_2(5)] = 190 \pm 60$ Å^2 and $\sigma[F_1(10)] = 110 \pm 30$ Å^2. The agreement between these values and the data presented in this study is within the combined error of the two measurements. However, the error in the previous measurements is too large to permit observation of a systematic variation of the RET rate with rotational level. In contrast, a monotonic decrease in the RET rate with increasing rotational energy has been observed in the current experiments.

The accuracy of the quenching rate measurement can also be examined. Cross sections for H_2O, H_2 and O_2 have been taken from Garland and Crosley [30] for the $v' = 0$, $N' = 7$ state, and the H-atom cross section is from Cattolica and Mataga [22]. The contribution of the other species to the quenching is insignificant. Combining these cross-sections with the flame composition results in a total quenching rate of 29×10^6 s^{-1}, the primary contributions coming from H_2O (69% of the total) and H (25% of the total). This rate compares well with our measurement of $28.9 \pm 0.5 \times 10^6$ s^{-1} for this level.

6 Error Analysis

The errors in the measurement of the RET rates are mostly due to uncertainties in the determination of the energy level populations. There are several sources for these uncertainties, and the most important error source is the relation of the broadband and narrowband fluorescence signals wia calibration with the fluorescence spectra. In the calibration process, several effects may contribute to the error. A detailed discussion of all error-sources is given below.

Successive scans over fluorescence transitions originating from the directly laser-coupled level were typically quite repeatable, with variations from scan-to-scan on the order of 1–4%. The exception is the study of the $F_2(12)$ level, where the excitation of the weak $S_1(10)$ transition led to an increased error. In addition for $N' \geq 10$ there is a residual systematic variation of approximately 8–10% in the relative strengths of the P, Q and R lines originating from the laser-coupled state, compared to the well-known transition probabilities. The

influence of this uncertainty on the determination of the RET rates has been reduced by using an averaged value for the LIF signal from the laser-excited state.

For some of the rotational levels, it was not possible to detect fluorescence lines from the directly laser-coupled state which were completely isolated from other transitions. Typically, the overlapping lines were weak satellites or transitions originating from high rotational quantum numbers, and thus the contribution of these lines was small. For measurement of lines in the P_2 and Q_2 branches, overlaps with satellites were estimated to increase the fluorescence signal originating from this state by $\approx 2\%$. For the other transitions, the magnitude of the effect was smaller.

Detection of the fluorescence from the $F_1(0)$ level is subject to several sources of error which are less significant for the other rotational levels. This is due to the fact that there are only two strong radiative transitions, $P_{12}(1)$ and $P_1(1)$, which are coupled to this level (the weak $O_{12}(2)$ line could not be detected). Excitation to $F_1(0)$ was performed via the $P_{12}(1)$ line, and detection of the fluorescence on the same transition is subject to two sources of interference: laser scattering and partial overlap with the $Q_2(6)/Q_{21}(6)$ transitions. The influence of $Q_2(6)/Q_{21}(6)$ overlap has been examined by measuring the $Q_1(6)/Q_{21}(6)$ lines, and has been estimated to be relatively small. In contrast, the contribution of laser scattering is difficult to determine accurately. Measurements performed with the laser tuned off-line have resulted in an estimated contribution to the signal of $\approx 50\%$, and the LIF signal has been corrected for this effect. However, the accuracy of this correction is unclear. The influence of laser scattering can be removed by detecting the $P_1(1)$ transition instead. However, this transition is closely overlapped by the $Q_1(3)/Q_{12}(3)$ line pair. The contribution of this line has been estimated from the $P_2(4)/P_{21}(4)$ line to be ≈ 20–30%. When the influence of these contributions to the $P_{21}(1)$ and $P_1(1)$ lines is included, the relative strengths of the lines differs from the expected ratio (determined from the Einstein A coefficients) by $\approx 30\%$. Since there it is not possible to determine which line strength has been more accurately measured, the averaged value has been used, leading to an estimated error in the fluorescence from the $F_1(0)$ state of $\pm 15\%$. This relatively large error leads to $\approx \pm 25\%$ uncertainty in the RET rate for this state.

The final source of error which must be considered is the determination of the RET rate via extrapolation to the beginning of the laser pulse. As shown in Fig. 6, the initial 10 ns of the laser excitation are not used for the extrapolation. This is because the determination of the population $N_c(t)$ by subtraction of the narrowband transient from the broadband transient is subject to large errors during the initial rise in the laser pulse, when the populations vary rapidly. Instead, the extrapolation is typically performed over a time scale ranging from 10 ns to 40 ns for $N' = 0$, 4 and 5, 10 to 50 ns for $N' = 7$, and 10 ns to 60 ns for $N' = 10$, 12 and 15. A longer extrapolation period can be used for the higher rotational levels, because the influence of back-transfer is smaller for these states. The results of the full multi-level model calcula-

tions discussed earlier show that initiating the extrapolation at 10 ns results in an error in the measured RET rate of $\approx 2\%$. The reduced back-transfer results in a smaller extrapolation error for the high-lying rotational states.

Note that errors may also be incurred when converting the measured energy transfer rates into cross sections. This conversion relies upon a calculation of the flame composition from a 1-D flame code [29], which in turn is influenced by the accuracy of the measured centerline temperature profile. Erroneous species concentrations will lead to systematic errors in the energy transfer cross sections. All studies of energy transfer where the gas composition is not directly measured share this problem to some degree, and estimation of the magnitude of this systematic error is difficult. It is anticipated that for the measurements presented here this error will be relatively small, since we have reasonable confidence in the accuracy of both the temperature measurement and the flame code calculations.

Exact determination of the species-specific RET cross sections for OH in collisions with H_2O requires knowledge of the contributions of He and H atoms to the RET. We have corrected the data for He RET using the calculations of Jörg et al. [15] when possible, and since no data on H-atom RET is available, we have not attempted to correct the measurements for this contribution. Other than the correction for He RET, the quoted errors for the cross sections do not reflect the possible influences of He and H atoms.

7 Summary

High-temperature total RET and quenching rates have been measured for a number of rotational levels in the $A^2\Sigma^+$, $v' = 0$ level of OH for collisions with H_2O. These results represent the first measurements of both OH RET and quenching rates at elevated temperature in the same study. Comparison of the data with previous measurements of RET and quenching illustrates good agreement. In addition, systematic decreases in the rates with increasing rotational quantum number are observed, the first time such an effect has been seen for OH RET at elevated temperature. The RET rate decreases more rapidly than the quenching rate with increasing rotational energy, a result which is consistent with previous measurements of the branching ratio Q/R.

References

1. R. Kienle, M.P. Lee, U. Meier, K. Kohse-Höinghaus: 3rd Int'l Symp. on Special Topics in Chemical Propulsion: Non-Intrusive Combustion Diagnostics, Scheveningen, The Netherlands (1993) R. Kienle, M.P. Lee, K. Kohse-Höinghaus: unpublished
2. R.K. Lengel, D.R. Crosley: J. Chem. Phys. **68**, 5309 (1978)
3. J. Burris, J.J. Butler, T.J. McGee, W.S. Heaps: Chem. Phys. **124**, 251 (1988)
4. A. Jörg, U. Meier, K. Kohse-Höinghaus: J. Chem. Phys. **93**, 8757 (1990)
5. J. Burris, J.J. Butler, T.J. McGee, W.S. Heaps: Chem. Phys. **151**, 233 (1991)
6. A. Jörg, U. Meier, R. Kienle, K. Kohse-Höinghaus: Appl. Phys. B **55**, 305 (1992)
7. R. Kienle, A. Jörg, K. Kohse-Höinghaus: Appl. Phys. B **56**, 249 (1993)
8. G.P. Smith, D.R. Crosley: *18th Symp. (Int'l) on Combustion* (The Combustion Institute, Pittsburgh, PA 1981) pp. 1511–1520
9. D. Stepowski, M.J. Cottereau: J. Chem. Phys. **74**, 6674 (1981)
10. Y. Furuya, M. Yamamoto, Y. Takubo: Jpn. J. Appl. Phys. **24**, 455 (1985)
11. R.P. Lucht, D.W. Sweeney, N.M. Laurendeau: Appl. Opt. **25**, 4086 (1986)
12. G. Zizak, J.A. Lanauze, J.D. Winefordner: Combust. Flame **65**, 203 (1986)
13. C. Chan, J.W. Daily: Appl. Opt. **19**, 1357 (1980)
14. A.D. Esposti, H.-J. Werner: J. Chem. Phys. **93**, 3351 (1990)
15. A. Jörg, A.D. Esposti, H.-J. Werner: J. Chem. Phys. **93**, 8757 (1990)
16. I.S. McDermid, J.B. Laudenslager: J. Chem. Phys. **76**, 1824 (1982)
17. R.A. Copeland, D.R. Crosley: Chem. Phys. Lett. **107**, 295 (1984)
18. R.A. Copeland, M.J. Dyer, D.R. Crosley: J. Chem. Phys. **82**, 4022 (1985)
19. R.A. Copeland, M.L. Wise, D.R. Crosley: J. Phys. Chem. **92**, 5710 (1988)
20. C.B. Cleveland, J.R. Wiesenfeld: Chem. Phys. Lett. **144**, 479 (1988)
21. J.B. Jeffries, K. Kohse-Höinghaus, G.P. Smith, R.A. Copeland, D.R. Crosley: Chem. Phys. Lett. **152**, 160 (1988)
22. R.J. Cattolica, T.G. Mataga: Chem. Phys. Lett. **182**, 623 (1991)
23. I.L. Chidsey, D.R. Crosley: J. Quant. Spectrosc. Radiat. Transfer **23**, 187 (1980)
24. A. Goldman, J.R. Gillis: J. Quant. Spectrosc. Radiat. Transfer **25**, 111 (1981).
25. M.R. Trolier: Kinetic and spectrosopic studies of ozone photochemistry. Ph. D. Thesis, Cornell University, Ithaca (1988)
26. E.H. Piepmeier: Spectrochim. Acta **27B**, 445 (1972)
27. A.C. Eckbreth: *Laser Diagnostics for Combustion Temperature and Species* (Abacus, Kent 1988)
28. D.H. Campbell: Appl. Opt. **23**, 1319 (1984)
29. J. Warnatz: Institut für Technische Verbrennung, Universität Stuttgart: One-dimensional flame code, 1991 version
30. N.L. Garland, D.R. Crosley: 21st Symp. *(Int'l) on Combustion* (The Combustion Institute, Pittsburgh, PA 1986) pp. 1693–1702
31. R. Kienle, T.A. Griffin, M.P. Lee, K. Kohse-Höinghaus: unpublished
32. J. Kiefer (ed.): *Ultraviolette Strahlen* (de Gruyter, Berlin 1977) p. 216
33. G.M. Dieke, H.M. Crosswhite: J. Quant. Spectrosc. Radiat. Transfer **2**, 97 (1962)
34. M.J. Dyer, D.R. Crosley: Opt. Lett. **14**, 12 (1989)
35. E.C., Rea, Jr., A.Y. Chang, R.K. Hanson: J. Quant. Spectrosc. Radiat. Transfer **41**, 29 (1989)